Spatial Enhancement of Event-Related Potentials Using Multiresolution Analysis

Kongming Wang*, Henri Begleiter*, and Bernice Porjesz*

Summary: Multiresolution analysis is a potentially useful tool to enhance the brain's electrical fields (spatial distributions of event-related potentials (ERP)), and to bring out spatial features which may not be seen in the fields before enhancement. For comparing different images (slices from ERP of different subjects or from the same subject but evoked by different stimuli), we define a measure (surface energy) at each decomposition scale and for different wavelets. The best wavelet and the best level for comparing the given images can be chosen based on this measure. Our experiments show that for very similar images, their difference can be brought out at some scale level. Three preprocessing steps are needed in order to carry out this wavelet analysis. First, a wavelet denoising step is needed to remove noise from the raw ERP. Secondly, a one-to-one mapping is needed to map scalp surface into a square, because the current wavelet analysis theory and algorithm are constructed on regular domains. Finally, a fitting or interpolation step is needed to construct an image on a regular grid in order to apply the fast wavelet transform algorithms.

Key words: ERP; Brain's electrical fields; Multiresolution analysis; Denoising; Local polynomial fitting; Wavelet.

Introduction

Characterizing the brain's electrical fields has been given a great deal of attention in electroencephalogram (EEG) and event-related potential (ERP) topography. Electric currents generated by sources in brain are volume conducted through brain, cerebrospinal fluid, skull, and scalp to the recording electrodes. Therefore, potentials measured at an electrode represent the summation of signals from many sources over the brain, especially when considering the signals of higher cognitive functions such as P3. The P3 component is a large positive deflection occuring at a latency of 300-500 msec after a stimulus of "significance" and is of maximum amplitude at the PZ electrode. In order to see the local topographic variations in neurocognitive processes, the recorded potentials need to be spatially enhanced (sharpened). Typically, this is done with surface Laplacian measures which provide reference-independent estimates of radial current source density (Le et al. 1994, Nunez et al. 1994) and eliminate common activity due to volume conduction from distant sources (Nunez 1995). We represent a surface (electric potentials) as surface = trend (linear and bilinear terms) + details.

Then the surface Laplacian removes the trend but keeps a transformed version (through Laplacian operator) of the details. Therefore the surface Laplacian is able to bring out spatial features which cannot be noted in evoked potentials.

In this paper, we use multiresolution analysis as a tool for performing the spatial enhancement of ERP. In multiresolution analysis, the orthogonal wavelet transform decomposes an image into independent information at different scale (spatial frequency) levels. For two images which are different at only one level, wavelet decomposition might bring out this difference while surface Laplacian may fail.

An immediate application of the multiresolution analysis is the comparison of the brain's electrical fields of different subjects (control, alcoholic) or the fields of a subject evoked by different stimuli. After decomposing each field into details at several levels, one can measure the difference at each level. The level with the biggest dispersion identifies the largest difference between the fields. We will measure a surface (field) by its energy. In our visual P3 studies, the amplitudes of the ERP of the control and alcoholic subjects are quite different (see figures 7 and 11), but the electrical fields at 400 msec (near P3) are similar. In fact, one cannot see the difference visually. The difference is brought out by multiresolu-

*Neurodynamics Laboratory, Department of Psychiatry, SUNY Health Science Center at Brooklyn, Brooklyn, New York, USA.

Accepted for publication: October 10, 1997.

We thank Arthur Stimus for providing the ERP data. This research is supported by N.I.H. grants AA 05524 and AA 02686 to HB.

Correspondence and reprint requests should be addressed to Kongming Wang, Neurodynamics Laboratory, Department of Psychiatry, SUNY Health Science Center at Brooklyn, 450 Clarkson Avenue, Brooklyn, NY 11203, USA.

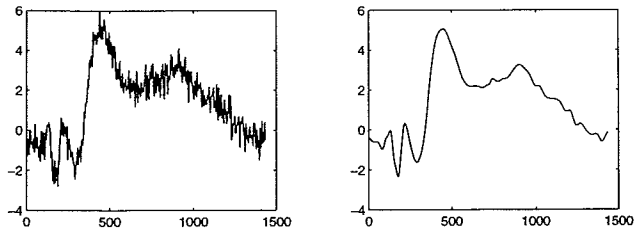

Figure 1. Noisy visual potential (left) and denoised version (right). Horizontal unit is in msec and vertical unit is in microvolts.

tion analysis. Similar results are obtained when comparing the electrical fields of a control subject evoked by different stimuli.

The drawback of the multiresolution analysis is that the brain's electrical fields have to be mapped onto images on a regular grid, because the international system for placing sensors on scalp does not match a regular grid. We will construct a one-to-one mapping of the scalp surface onto a square, keeping image distortion as small as possible. We will then apply local polynomial fitting to construct approximate images on a regular grid. To reduce error propagation, noise is removed by wavelet denoising from the raw data.

Methods

Wavelet denoising

We assume an additive noise model

$$s_{ij}(t) = p_{ij}(t) + \sigma_{ij}\, n_{ij}(t) \qquad (1)$$

where $s_{ij}(t)$ is the evoked potential with stimuli i and recorded at sensor j and at time t, $p_{ij}(t)$ is the true but unobserved potential, $n_{ij}(t)$ is a Gaussian white noise $N(0,1)$ which represents the human and instrument errors, and σ_{ij} is the unknown noise level (standard deviation). Wavelet denoising consists of three steps. In order to simplify the notation, we will omit the subscripts ij, because they are fixed throughout the denoising process.

1. Wavelet decomposition of s. Choose a wavelet ψ and a decomposition level N. Wavelet coefficients of s are computed by

$$w(a, b) = \langle s, \psi_{a,b} \rangle = \langle p, \psi_{a,b} \rangle + \sigma \langle n, \psi_{a,b} \rangle \qquad (2)$$

Here $a=1, \cdots, N$ is the scale parameter and b is the location parameter. We will use the wavelet "sym8" (Symlets of order 8, near symmetric, smooth, compact support). For details about wavelet families, see Meyer (1993) and Misiti et al. (1996). Note that many wavelet families do not have an explicit expression.

2. Shrinking wavelet coefficients. If p is a smooth (lower frequency) signal, then the wavelet decomposition of p at the finest level (a=1, high-pass filtered) yields almost zero coefficients. This is because ψ has several vanishing moments. Therefore $w(1,b) \approx \sigma \langle n, \psi_{1,b} \rangle$. But orthogonal transform of Gaussian white noise n yields again Gaussian white noise $\langle n, \psi_{1,b} \rangle$. We see that the median absolute deviation of $\{w(1,b)\}$ is a robust estimate of σ. Equation (2) implies that by shrinking the wavelet coefficients $w(a,b)$ towards zero, one can remove noise from the signal. Many shrinking methods have been proposed in the wavelet literature. We use a mixture rule of Stein's unbiased risk estimate and a fixed form threshold $\sqrt{2 \log (\text{length(s)})}$. For more details, see Misiti et al. (1996).

3. Reconstruction. Compute the denoised signal from the modified wavelet coefficients by the inverse wavelet transform.

Figure 1 depicts a signal and the denoised version. It shows that wavelet denoising is quite efficient. For non-Gaussian noise, a nonlinear wavelet shrinkage (different amounts of shrinkage at different decomposition scales) should be applied to remove noise.

The mapping of scalp surface to a square

Most wavelets for function analysis are constructed in $\mathbf{R}^n$ and fast algorithms are implemented for regular domains such as interval (n=1) and square (n=2). Human scalp surface is not such a regular domain. In this paper we assume a two dimensional disk scalp surface. A half sphere scalp surface is mapped to a disk by the simple projection $(x,y,z) \mapsto (x,y)$ without image distortion.

One way of transforming data from the scalp surface to an image in a regular domain is to find the smallest square containing the scalp surface. Then the interpolation-prediction is used to construct an image on a regular grid. Interpolation is not a problem, because the noise has been removed in the previous step. But the prediction would give a poor approximation at the corners, because there is no data point near there. We will construct a one-to-one mapping from a scalp surface to a square with the following three properties:

1. Image distortion as small as possible. This means that uniformly distributed points should be mapped to almost uniformly distributed points. Note that this property disqualifies polar parametrization (see figure 2).

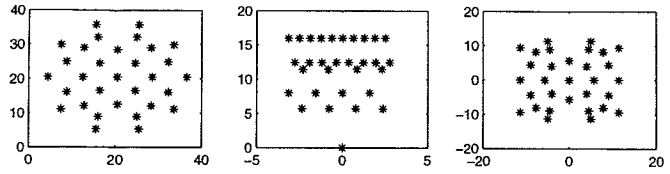

Figure 2. Sensor locations on scalp (left), polar parametrization (middle) where the center of the scalp is mapped to (0,0), and mapped locations in a square (right) where the center of the scalp is mapped to (0,0).

2. One-to-one mapping. Analyzed images in a square can be converted back to images on a scalp surface.

3. Smooth mapping. Mapping should be smooth so that the results from other tools such as surface Laplacian can be converted back and forth.

We will use the following mapping from the scalp surface to a square:

$$(x,y)\mapsto(u,v), \quad \text{if} \quad y>|x|$$

where

$$u=x, \quad v=\frac{r_3}{r_1}r_2+|x|,$$

$$r_1=\sqrt{r^2-x^2}-|x|, \quad r_2=y-|x|, \quad r_3=\frac{\sqrt{2}}{2}r-|x|,$$

and r is the radius of the scalp surface. The mapping of other parts of the scalp surface $-y>|x|, x>|y|, -x>|y|$ is constructed similarly with symmetry. The idea is to divide the scalp surface into four cones equally, and shrink each cone to a triangle towards the center of the scalp surface. The edges of the cones are kept unchanged. The mapping of 31 electrode locations is given by figure 2.

Local polynomial fitting

To apply wavelet techniques, we need to evaluate potentials on a regular grid (square lattice in our case). The international system for placing sensors on the scalp does not match this regular grid. We will apply local polynomial fitting to estimate potentials at each point of a square lattice.

Let $s_i(x_{j1}, x_{j2}, t)$ be the brain potential evoked by stimulus i and recorded at location (x_{j1}, x_{j2}) and time t. We will omit subscripts i,t in this section because they are fixed throughout the estimation process. We assume an additive noise model for the scalp electrical fields

$$s(x_{j1}, x_{j2}) = p(x_{j1}, x_{j2}) + \varepsilon_j, \tag{3}$$

where p is the true but unobserved potential and ε is a residual term with mean zero. Note that (3) is a spatial model while model (1) is a time series. Even though a wavelet denoising operation has been performed for signals from each sensor, data are still noisy. First, any denoising operation cannot remove noise completely. Secondly, sensors are placed on the scalp with random errors which have no effect on the model (1).

In a neighborhood of a grid point (u_1, u_2), Taylor expansion gives

$$p(x_1,x_2)=a_0+a_1(x_1-u_1)+a_2(x_2-u_2)+\frac{a_3}{2}(x_1-u_1)^2+$$
$$a_4(x_1-u_1)(x_2-u_2)+\frac{a_5}{2}(x_2-u_2)^2+\cdots$$

with $p(u_1, u_2) = a_0$. Estimation of a_0 will be based on a quadratic model

$$p(x_1,x_2)\approx p_2(x_1-u_1,x_2-u_2,a)\equiv$$
$$a_0+a_1(x_1-u_1)+a_2(x_2-u_2)+\frac{1}{2}a_3(x_1-u_1)^2+$$
$$a_4(x_1-u_1)(x_2-u_2)+\frac{1}{2}a_5(x_2-u_2)^2$$

with $a = (a_0, \cdots, a_5)$.

Let $\hat{a}_i, i=0,\cdots,5$, be the minimizer of the weighted least square problem

$$\min_a \sum_{j=1}^{m} W_h(x_{j1},x_{j2},u_1,u_2)(s(x_{j1},x_{j2})-p_2(x_{j1}-u_1,x_{j2}-u_2,a))^2$$

Here

$$W_h(x_{j1},x_{j2},u_1,u_2)=W\left(\frac{\|(x_{j1},x_{j2})-(u_1,u_2)\|}{h}\right)$$

with a spherically symmetric weight function W: $W(0)=1$, $W(r)=0$ for $r\geq 1$, and W is decreasing on the interval $[0,1]$. The bandwidth h determines how many data points are used in estimating the local polynomial and the proper weights assigned to each data point. We have

$$p(u_1,u_2)\approx\hat{a}_0$$

Repeating this procedure for every point (u_1, u_2) of a

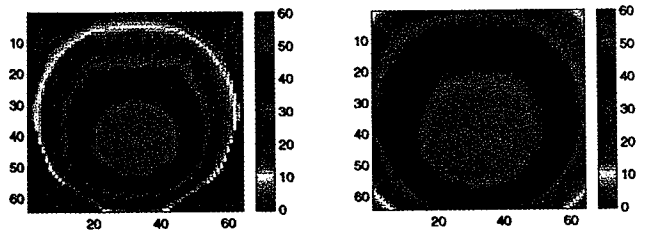

Figure 3. Visually evoked potentials (left, at 400 msec) constructed with interpolation, and mapped image in a square (right) by local polynomial fitting (first map scalp potentials into a square, then construct the image on a regular grid by local polynomial fitting). The size of both images are 64 by 64 points.

regular grid, we obtain an image on the regular grid. See figure 3 for an illustration.

The crucial issue in local polynomial fitting is how to choose bandwidth h. A larger h reduces variance of the estimator $\hat{a}_i, i = 0, \cdots, 5$, and increases their bias. On the other hand, a smaller h reduces bias and increases variance. Intuitively, higher noise levels require a larger bandwidth h because more data points are needed to reduce the variance of $\hat{a}_i$ (central limit theorem). Many procedures like cross-validation have been proposed for selecting h. We will simply choose h to be as small as possible such that the minimization problem is well-defined (as long as enough data points are used, the minimization problem is well defined). This is justified because of the wavelet denoising step and because the error of placing electrodes is small. For more details about local polynomial fitting, see Loader (1996). From now on, the brain's electric fields are plotted using the following direction: top — front head; bottom — back head; left — left head; and right — right head.

Multiresolution analysis

The one dimensional wavelet decomposition of signals consists of a high-pass filter and a low-pass filter at each scale level. The high-pass filter produces details of a signal at this level, while the low-pass filter gives the trend of a signal at this level.

It is similar in two dimensional wavelet analysis of images. There exist four functions $\phi_0(x_1,x_2)$, $\psi_1(x_1,x_2)$, $\psi_2(x_1,x_2)$, $\psi_3(x_1,x_2)$ such that the following four sequences

$$2^k \phi_0 (2^k x_1 - k_1, 2^k x_2 - k_2), \quad 2^j\psi_1(2^j x_1 - k_1, 2^j x_2 - k_2),$$

$$2^j \psi_2 (2^j x_1 - k_1, 2^j x_2 - k_2), \quad 2^j\psi_3(2^j x_1 - k_1, 2^j x_2 - k_2),$$

$k_1, k_2 \in \mathbf{Z}$ and $j \geq k$, form an orthonormal basis of $L^2(\mathbf{R}^2)$ for any given $k \geq 0$. Here $L^2(\mathbf{R}^2)$ is the set of square integrable functions on the plane. For details, see Meyer (1993).

We will use a one dimensional wavelet, and construct a two dimensional wavelet by tensor product. Let (ϕ, ψ) be a one dimensional father (low-pass filter) and mother (high-pass filter) wavelet pair. Then we take

$$\phi_0(x_1,x_2)=\phi(x_1)\,\phi(x_2), \quad \psi_1(x_1,x_2)=\phi(x_2)\,\psi(x_1),$$

$$\psi_2(x_1,x_2)=\phi(x_1)\,\psi(x_2), \quad \psi_3(x_1,x_2)=\psi(x_1)\,\psi(x_2),$$

Now at each scale level j, a given image f is decomposed into four sub-images with wavelet coefficients:

1. Trend (or: approximation) at scale level j (low-pass filtered in both dimensions).

$$2^j \int f(x_1,x_2)\phi_0(2^j x_1 - k_1, 2^j x_2 - k_2)dx_1dx_2, \quad k_1,k_2 \in \mathbf{Z}$$

2. Horizontal details at scale level j (low-pass filtered in dimension 2 while high-pass filtered in dimension 1).

$$2^j \int f(x_1,x_2)\psi_1(2^j x_1 - k_1, 2^j x_2 - k_2)dx_1dx_2, \quad k_1,k_2, \in \mathbf{Z}$$

3. Vertical details at scale level j (low-pass filtered in dimension 1 while high-pass filtered in dimension 2).

$$2^j \int f(x_1,x_2)\psi_2(2^j x_1 - k_1, 2^j x_2 - k_2)dx_1dx_2, \quad k_1,k_2 \in \mathbf{Z}$$

4. Diagonal details at scale level j (high-pass filtered in both dimensions).

$$2^j \int f(x_1,x_2)\psi_3(2^j x_1 - k_1, 2^j x_2 - k_2)dx_1dx_2, \quad k_1,k_2 \in \mathbf{Z}$$

Let f be a given image. Then f can be reconstructed from the wavelet coefficients as

$$\begin{aligned} f(x_1,x_2) = {} & \text{trend at scale level } 0 + \\ & + \text{three detailed images at scale level } 0 + \\ & + \text{three detailed images at scale level } 1 + \\ & + \text{three detailed images at scale level } 2 + \\ & + \cdots \end{aligned} \tag{4}$$

Since this decomposition is orthogonal, we see that the image is decomposed by wavelet analysis into information (trend at level 0 and fluctuations at each scale level j) that is independent from one scale to another. If we want to look at the trend and details at scale level N, then

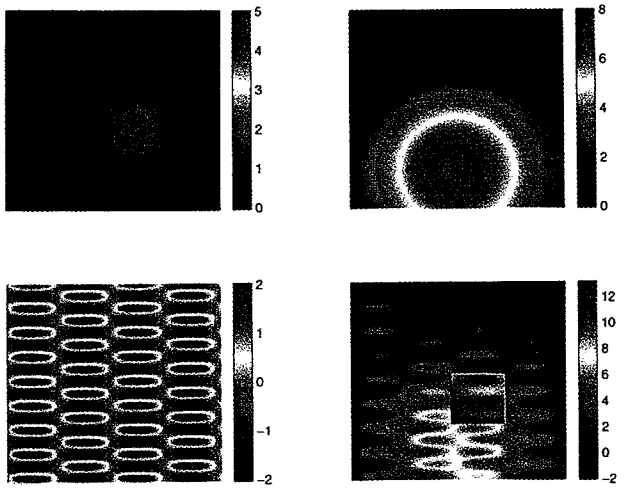

Figure 4. Three components and their mixture image (bottom-right).

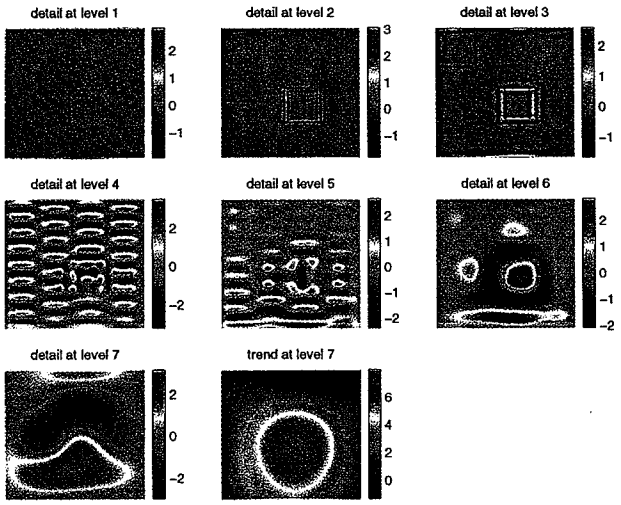

Figure 5. Wavelet decomposition of the image in figure 4. The wavelet "sym8" is used.

$$
\begin{aligned}
f(x_1,x_2) = {} & \text{trend at scale level } N + \\
& + \text{three detailed images at scale level } N + \\
& + \text{three detailed images at scale level } (N+1) + \\
& + \text{three detailed images at scale level } (N+2) + \\
& + \cdots
\end{aligned} \tag{5}
$$

where

$$
\begin{aligned}
\text{trend at scale level } N = {} & \text{trend at scale level } 0 + \\
& + \text{three detailed images at scale level } 0 + \\
& + \cdots \\
& + \text{three detailed images at scale level } (N-1).
\end{aligned} \tag{6}
$$

This is a multiresolution analysis of two dimensional images.

The discrete wavelet decomposition starts from the finest level (see Misiti et al. 1996). After decomposition at the finest level, one has four images: the trend and three details. Next one decomposes the trend of the present level to get the trend and three details at the next level. Because of the dyadic structure of the wavelet decomposition, there is a limit on how many levels wavelet decomposition can attain.

Another consideration is how to choose a proper wavelet for such multiresolution analysis. Many wavelet families have been constructed in the literature. The idea is that a less smooth wavelet should be chosen if the image is rough, and a smoother wavelet should be chosen if the image is smoother. If one chooses a smooth wavelet for a rough image, one would not see some details because they are smoothed out. On the other hand, if one chooses a rough wavelet for a smooth image, one could create some artificial bumps. We will use the wavelet "sym8" (Symlets of order 8) in the example of this section, because we have a smooth image.

Since a wavelet decomposition is a linear operation, it is easy to manipulate the decomposition for different purposes. We will add the details at each level and obtain a decomposition similar to a wavelet decomposition in dimension one. That is, an image is decomposed into two images (trend and detail) at each level rather than four images.

Figure 4 depicts an image which is the sum of three components with different spatial distributions. The first component consists of two squares. The second one is a smooth image of lower spatial frequency. The last one is also smooth but is of higher spatial frequency. Wavelet decomposition of this image is plotted in figure 5. Again wavelet "sym8" is used. At the finest levels (levels 1-3) the boundary of the two squares are captured even though the square at the top-left corner is almost invisible. Details at levels 4 and 5 are basically the higher frequency image (the third component). Details at level 6 show a square of the first component. The other square is not enhanced because of its lower intensity. Details at level 7 are part of the second component. The trend is the sum of the lower frequency images of all three components.

Comparing the brain's electrical fields

The importance of wavelet analysis is that at each

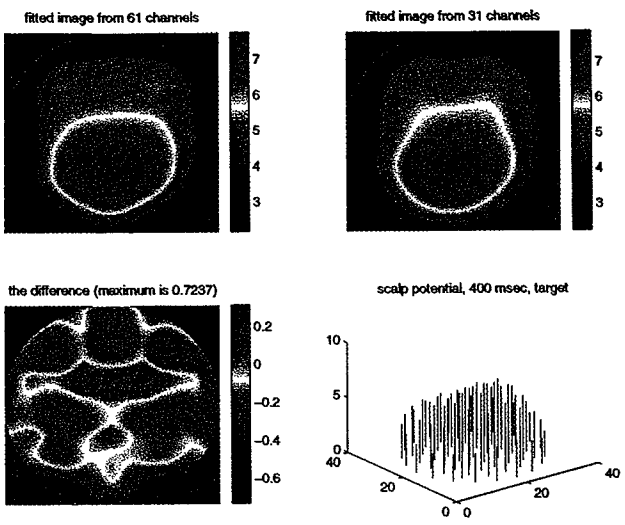

Figure 6. Fitted images based on data of 31 and 61 channels respectively. The difference of the two fitted images are also plotted.

decomposition level one can tell the difference between potentials recorded from the same head but evoked by different stimuli, or between potentials recorded from different heads (e.g., control and treatment subjects). While graphics can show this difference visually, quantitative analysis provides means to measure the difference at each level, and hence to pick up the most interesting scale level at which one can see the biggest difference of potentials from different heads. For this purpose, some descriptive parameters of an image need to be defined.

A global measure is the surface energy. Recall that for a surface f on $\mathbf{R}^2$, its surface energy is defined by

$$E(f)=\int\left[f(x_1,x_2)\right]^2 dx_1 dx_2.$$

In order to compare M images of the same size, we decompose each image at N scale levels. For images of different size, an interpolation step can be used to construct images with the same size. At level j, the image i is decomposed into two sub-images f_{ij}^a (trend or approximation) and f_{ij}^d (total detail). Define the difference measure between the M images at level j by

$$D_j=\sum_{1\le k<i\le M}\left[E\left(\frac{f_{ij}^a}{\|f\|_{ij}^a}-\frac{f_{kj}^a}{\|f\|_{kj}^a}\right)+E\left(\frac{f_{ij}^d}{\|f\|_{ij}^d}-\frac{f_{kj}^d}{\|f\|_{kj}^d}\right)\right]. \quad (7)$$

Then the largest difference between these images lies in level j_0, where j_0 is such that

$$D_{j_0}=\max_{1\le j\le N} D_j.$$

The normalization in (7) is by supernorm. That is,

$$\|f\|_{ij}^a=\max_{x_1,x_2}\left|f_{ij}^a(x_1,x_2)\right|.$$

By normalizing, we consider two images $f(x_1,x_2)$ and $cf(x_1,x_2)$ to be the same for all $c>0$, because they have exactly the same spatial distribution.

Note that this surface energy measure is wavelet dependent. For different wavelets, the maximum difference may occur at different decomposition levels. This is easy to understand because different wavelets have different shapes and vanishing moments. For a given image, one can compute the difference measure D_j^ψ for different wavelets ψ and at different scale levels j. Then the best wavelet ψ_0 and the best scale level j_0 for comparing the M images are given by the solution of the following optimization problem

$$D_{j_0}^{\psi_0}=\max_{\{\psi\},\,1\le j\le N} D_j^\psi.$$

We have used a global measure (surface energy) to select a wavelet and a decomposition level for comparing different images. Other measures can also be employed. For example, let $D_j=D_j^a+D_j^d$ where

$$D_j^a=\sum_{1\le k<i\le M} E\left(\frac{f_{ij}^a}{\|f\|_{ij}^a}-\frac{f_{kj}^a}{\|f\|_{kj}^a}\right).$$

Then $\{D_j^a\}$ can be used to select a wavelet and a decomposition level for comparing approximation (trend), while $\{D_j^d\}$ can be used for comparing details.

The ERP from different subjects may be recorded from different numbers of electrodes. To compare them, we need to construct images of the same size by local polynomial fitting. The number of electrodes affects the accuracy of the fitting. A more accurate estimate of the potential image is obtained with more electrodes. Figure 6 shows the fitted images from 31 and 61 electrodes respectively. The bars in the bottom-right graph represent the intensities of ERP recorded from 61 electrodes, where the 31 red bars indicate the channels used for fitting the top-right image. The maximum difference of

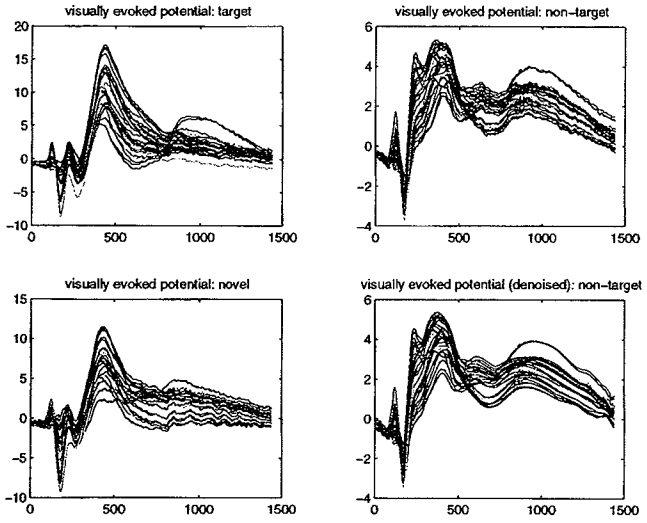

Figure 7. Plot of raw data recorded from 31 electrodes. Denoised potentials (non-target) are also plotted. Horizontal unit is in msec and vertical unit is in microvolts.

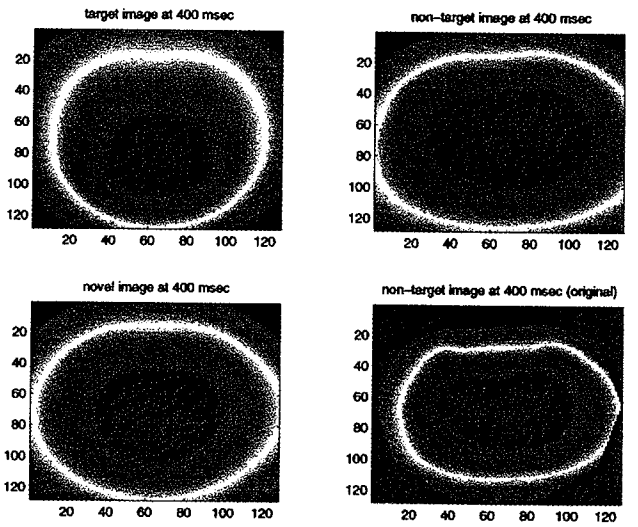

Figure 8. Mapped images in a square. ERP evoked by non-target stimuli are also plotted. Each image is scaled to full color scale. If all images are plotted in a fixed color scale, then no feature can be seen from the field evoked by non-target stimuli because of its relatively small amplitude.

the two fitted images is 0.7237 microvolts, which occurs at the boundary of the images. Overall the difference is small, less than 0.4 microvolts (see the bottom-left graph of figure 6).

Analyzing potentials evoked by different stimuli

Data collection

We recorded the visual P3 ERP in control subjects. Evoked potentials are recorded from 33 electrodes (31 electrodes of standard international recording system and two additional electrodes for monitoring eye movements). Subjects are presented with 280 visual stimuli with an ISI of 1.6 seconds. There are 210 non-target stimuli in the shape of a square, 35 target stimuli in the shape of an X, and 35 novel stimuli each a different colored polygon or other geometrical figure. Artifact threshold is set at 75 microvolts, the sampling interval is 3.906 milliseconds, and post-stimuli sample size is 368. After rejecting trials with artifacts, the average ERPs are obtained across trials. Then the noise is removed by wavelet shrinkage described in the previous section. The average data are plotted in figure 7.

We carry out a spatial wavelet analysis of the brain's electrical fields at 400 msec, a time consistent with the P3. Repeating this analysis process at consecutive time points provides major insights into the evolution of the brain's electrical fields.

The locations of the 31 sensors are mapped to points in a square by the one-to-one mapping technique described in the previous section. Then local polynomial fitting is employed to fit a 128 by 128 image on a regular grid. The constructed images are plotted in figure 8.

Wavelet decomposition

Each image is decomposed at 6 levels using wavelet "sym8". Recall that the information extracted at different levels are independent. Therefore by comparing the information from different images at each level, one is able to see the difference at some level of the decomposition even though the original images look pretty much the same (figure 8). The decomposition result is plotted in figure 9. As in the last section, we plot only the total details at each level. Since the images are smooth, there are no obvious features in the details of the first few scale levels. Therefore only the details at the last two scale levels and the trend at the last level are plotted. Recall that if we put together the details at all levels and the trend at the last level, we recover the original image.

Comparison results

We see from figure 9 that the details at levels 5-6 are different for different stimulus conditions. We will compute the difference measure D_j defined in the last section to confirm this difference. To see the effects of different wavelets, we compute D_j for Daubechies wavelets of

Table I. Surface energy D_j using Daubechies wavelets of different order. Last line is the difference of original images.

D_j	*db2*	*db4*	*db6*	*db8*	*db10*	*db12*	*db14*	*db16*
j=1	0.1125	0.1132	0.1102	0.1220	0.1147	0.1122	0.1135	0.1188
2	0.1093	0.1421	0.1110	0.1307	0.1220	0.1196	0.1220	0.1226
3	0.1084	0.1303	0.1374	0.1414	0.1477	0.1444	0.1517	0.1792
4	0.1232	0.1928	0.1860	0.1563	0.1993	0.1860	0.1483	0.1731
5	0.1031	0.2935	0.1185	0.2578	0.2070	0.2017	0.2781	0.2003
6	0.0403	0.4667	0.0707	0.7429	0.0957	0.6134	0.1373	0.4873
D_0	0.1007	0.1007	0.1007	0.1007	0.1007	0.1007	0.1007	0.1007

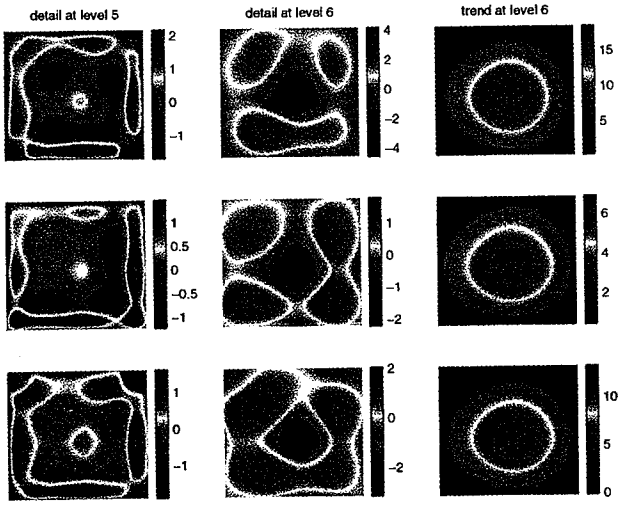

Figure 9. Decomposition of the target image (top row), non-target image (middle row), and novel image (bottom row) at 400 msec. The original images are plotted in figure 8. Details at the first four levels are omitted because no features can be seen. The images are plotted with the following direction: top — front head; bottom — back head; left — left head; and right — right head.

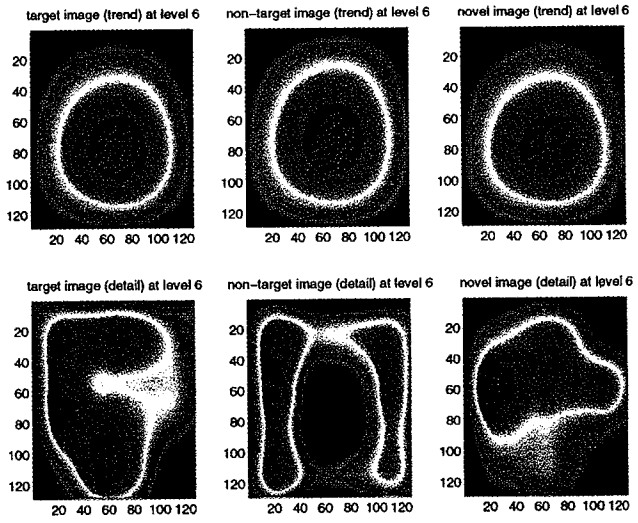

Figure 10. Decomposition of evoked potentials at 400 msec using Daubechies wavelet of order 8. The units give the image size (128 by 128 points).

order 2, 4, · · ·, 16 and for scale levels j=1, · · ·, 6. Results are grouped in table I. The difference measure of the original images is also tabled in the last line of table I for comparison. It is computed as

$$D_0 = E\left(\frac{I_t}{\|I_t\|} - \frac{I_{nt}}{\|I_{nt}\|}\right) + E\left(\frac{I_t}{\|I_t\|} - \frac{I_n}{\|I_n\|}\right) + E\left(\frac{I_n}{\|I_n\|} - \frac{I_{nt}}{\|I_{nt}\|}\right)$$

where I_t, I_{nt}, I_n are the target, not-target, and novel images. For an image f on a grid $\{ij\}$, we simply compute an equivalent surface energy

$$E(f) = \text{average of } \{ [f(i,j)]^2 \}.$$

Since the largest difference D_j is obtained with wavelet "db8" at level j=6, we see that Daubechies wavelet of order 8 should be used if we want to compare these three similar (D_0=0.1) images using a Daubechies wavelet. Figure 10 plots the three decompositions at level 6 using Daubechies wavelet of order 8.

Comparing the details of figure 10 and details of figure 9 at level 6, one can see that "sym8" and "db8" bring out different details from the recorded potentials. The reason is that the details of figure 10 at level 6 and the details of figure 9 at level 6 have different spatial frequencies, due to the different frequencies of the wavelets "sym8" and "db8". For comparing images, the same wavelet should be used for decomposing all images.

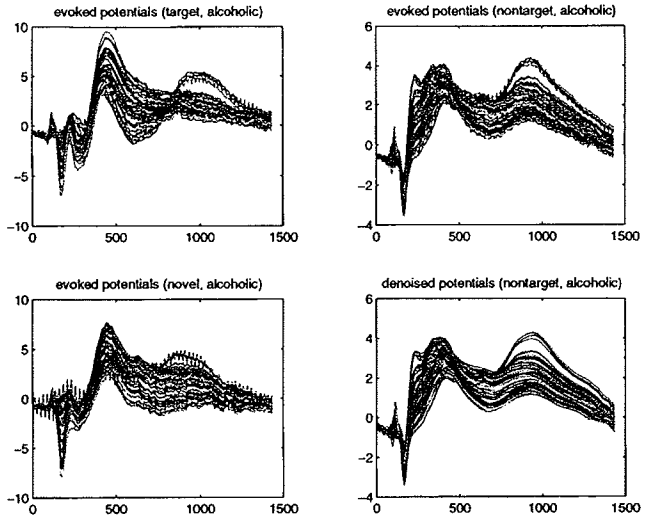

Figure 11. Plot of raw potentials of an alcoholic subject. Denoised potentials (non-target) are also plotted.

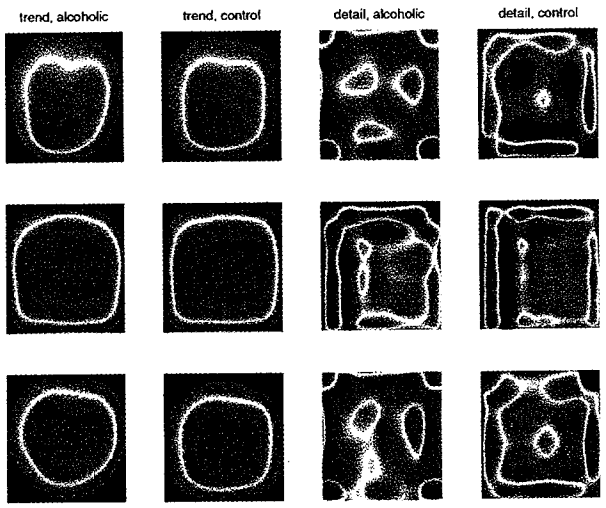

Figure 12. Plot of the wavelet decomposition (level 5) of potentials evoked by target stimuli (top row), non-target stimuli (middle row), and novel stimuli (bottom row). The images are plotted with the following direction: top — front head; bottom — back head; left — left head; and right — right head.

Comparing brain's electrical fields of control and alcoholic subjects

Data collection

Data from control subjects are described in the previous section. We will compare these ERP data with evoked potentials of alcoholic subjects. The experiment for recording evoked potentials is the same for both alcoholic and control subjects, except that potentials are recorded from 64 sensors (standard international system) for alcoholic subjects. Three sensors are for monitoring eye movements. Therefore we have a data set of 61 channels and 368 sample points. The raw data are plotted in figure 11.

Comparing figure 11 with figure 7, we see that the evoked potentials of control and alcoholic subjects have a similar shape, but the amplitudes of potentials of alcoholic subjects are considerably smaller. Our interest is to determine whether they are different spatially.

Again we cut a slice at 400 msec from each of the three traces. After preprocessing the data of alcoholic subjects (denoising, mapping to a square, and constructing 128 by 128 images with local polynomial fitting), we pair them with the slices from control subjects according to stimulus condition (target, non-target, novel). Then we analyze each pair as in the last section.

For each pair, we compute the surface energy of their difference: 0.0101 for target pair, 0.0021 for non-target pair, and 0.0230 for novel pair. This means that their spatial distribution is about the same for each pair even though their amplitude is quite different. From the recorded potential fields we cannot determine the difference in their spatial distributions.

After wavelet decomposition, the spatial difference between evoked potentials of control and alcoholic subjects is brought out at some scale level. Using the notation D_j of the last section with M=2, we find that D_5=0.0667 for target pairs using wavelet "sym8"; D_5=0.0350 for non-target pairs using wavelet "sym7" (Symlets of order 7); and D_5=0.0738 for novel pairs using wavelet "sym8". In terms of surface energy, images are sharpened by a factor of 3 to 6 at a scale level 5. The decompositions are plotted in the next figure. From the columns 3 and 4 of the figure 12, we see that significant spatial differences emerge between alcoholics and controls after wavelet decomposition.

Discussion

We have seen that multiresolution analysis is a potentially useful tool for spatially enhancing evoked potentials, mainly because it decomposes an image into independent information at different scale levels. This is particularly useful for extracting features from images, and hence for comparison studies of the brain's electric fields of different subjects.

Decomposing potential surfaces at consecutive time points, one is able to see the evolution of potential surface at each scale level. This is straightforward and we do not perform it in this paper.

The present implementation of fast wavelet transforms requires that images are defined in a regular grid and image size in each dimension has length 2^J for an integer J. For analyzing brain potentials, raw data have to be preprocessed (one-to-one mapping, local polynomial

fitting) before wavelet techniques can be employed.

A drawback of the implemented fast wavelet transforms is the boundary effects. Since both high-pass and low-pass filters of a wavelet transform have length greater than 1, boundary effects need to be considered. This means that different filters should be used when wavelet transform takes place near a boundary, and further work is needed.

References

Le, J., Menon, V., and Gevins, A. Local estimate of surface Laplacian derivation on a realistically shaped scalp surface and its performance on noisy data. Electroencephalography and Clinical Neurophysiology, 1994, 92: 433-441.

Loader, C. Local Regression and Likelihood: A guide to the LOCFIT software. http://cm.bell-labs.com:80/cm/ms/departments/sia/project/locfit/, 1996.

Meyer, Y. Wavelets Algorithms and Applications. SIAM, Philadelphia, 1993.

Misiti, M., Misiti, Y., Oppenheim, G., and Poggi, J.M. Wavelet TOOLBOX. The MathWorks, Inc., 1996.

Nunez, P.L. Neocortical Dynamics and Human EEG Rhythms. Oxford University Press, New York, 1995.

Nunez, P.L., Silberstein, R.B., Cadusch, P.J., Wijesinghe, R.S., Westdrop, A.F., and Srinivasan, R. A theoretical and experimental study of hign resolution EEG based on surface Laplacians and cortical imaging. Electroencephalography and Clinical Neurophysiology, 1994, 90: 40-57.